

Statistical Properties of Target Localization Using Passive Radar Systems

Mats Viberg

Blekinge Institute of Technology
Karlskrona, Sweden

Daniele Gerosa

Chalmers University of Technology
Göteborg, Sweden

Tomas McKelvey

Chalmers University of Technology
Göteborg, Sweden

Thomas Eriksson

Chalmers University of Technology
Göteborg, Sweden

Abstract—Passive Radar Systems have received tremendous attention during the past few decades, due to their low cost and ability to remain covert during operation. Such systems do not transmit any energy themselves, but rely on a so-called Illuminator-of-Opportunity (IO), for example a commercial TV station. A network of Receiving Nodes (RN) receive the direct signal as well as reflections from possible targets. The RNs transmit information to a Central Node (CN), that performs the final target detection, localization and tracking.

A large number of methods and algorithms for target detection and localization have been proposed in the literature. In the present contribution, the focus is on the seminal Extended Cancelation Algorithm (ECA), in which each RN estimates target parameters after canceling interference from the direct-path as well as clutter from unwanted stationary objects. This is done by exploiting a separate Reference Channel (RC), which captures the IO signal without interference apart from receiver noise.

We derive the statistical properties of the ECA parameter estimates under the assumption of a high Signal-to-Noise Ratio (SNR), and we give a sufficient condition for the SNR in the RC to enable statistically efficient estimates. The theoretical results are corroborated through computer simulations, which show that the theory agrees well with empirical results above a certain SNR threshold. The results can be used to predict the performance of passive radar systems in given scenarios, which is useful for feasibility studies as well as system design.

I. INTRODUCTION

The idea of employing illuminators of opportunity (IOs) like frequency modulation (FM) radio or television stations to perform radar tasks is not new, and it goes back at the very least to the successful experiment carried out by sir Robert Watson-Watt in 1935, who used the shortwave BBC Empire transmitter at Daventry (England) to detect a slow bomber aircraft at short distance [1]. This technique was later exploited by Germany since 1943, via the “Klein Heidelberg” receivers that used British active radar waveforms to detect incoming aircrafts across the Channel [1]. Despite the hardware technology being available since almost a century, the systems theoretical analysis using modern statistical signal processing language came later, and it is still subject to constant and ongoing investigation, which is in turn also partially sustained by actual deployments in ongoing conflicts (cfr. e.g. Ukraine’s *Kolchuga* passive reconnaissance radar [2]).

The research was funded by the strategic innovation programme “Smartare Elektroniksystem”, a joint research project financed by VINNOVA, Formas and the Swedish Energy Agency, and by SAAB.

Mats Viberg is also with Chalmers University of Technology.

Mathematical models utilized to describe passive radars vary depending on the task that the system is supposed to perform; for instance in *detection* applications the sensing waveform could be assumed to be fully unknown. The hypothesis testing is then cast as deciding whether *structure* (as opposed to randomness) is detected by the receiver nodes (RNs) [3]–[7]. Nevertheless, in many publications, detection is performed by exploiting a reference signal [8]. The situation is different in systems tasked to perform localization and / or radial velocity estimation; in those, RNs are usually assumed to have at least one reference channel (RC), dedicated to the reception of a strong line-of-sight signal with negligible clutter and target reflections [9]–[11], which is in turn actively used in processing the data received by the surveillance channel (SC). This is also the case considered in the present contribution. We are mainly concerned with the problem of estimating the target parameters, which may later be leveraged in a Generalized Likelihood Ratio Test (GLRT) for solving the detection problem, see e.g. [12]–[14].

The main contributions in this paper concern the statistical performance in terms of Mean-Square-Error (MSE) of the parameter estimates. The Cramér-Rao Lower Bound (CRLB) on the MSE has been studied in e.g. [15]–[17]. These are applicable when the reference signal is perfectly known. In contrast, [18] considers the case where an RC is unavailable and the reference signal is estimated jointly with the target parameters. Further, we are concerned with the case where the target reflections arriving at the SCs are obscured by direct path interference (DPI) from the IO received through the antenna sidelobes [19], as well as clutter that originates from the ground or stationary objects in the terrain. Both impairments may severely impact the accuracy of the estimation of targets’ parameters, and therefore different techniques have been developed to mitigate their effects [9], [10], [20]–[25].

In the present paper we rigorously analyze the performance of a Maximum Likelihood-type Estimator of the target velocity and position based on the Extensive Cancellation Algorithm (ECA) [9]. This leads to a compact CRLB formula and an expression for the MSE when noise in the reference channel is also accounted for. The analysis includes a study of uniqueness and consistency of the estimated parameters.

Specifically, the novel contributions are the following:

- 1) An interpretation of the Extensive Cancellation Algorithm (ECA) of [9] as an approximate Maximum Like-

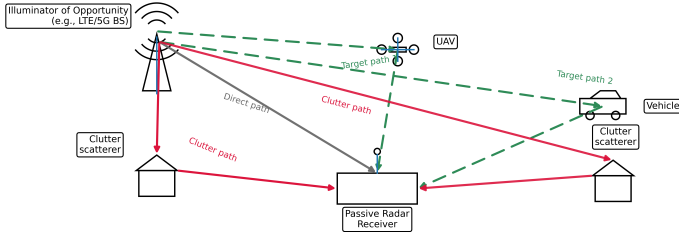


Fig. 1: General Passive Radar Geometry

lihood technique.

- 2) A proof of parameter identifiability and consistency of the parameter estimates for a class of stochastic processes.
- 3) A high-SNR analysis of the ECA estimates of the delay/Doppler parameters and/or the target location and velocity. An explicit expression of the covariance matrix of the estimation error is given, and it is interpreted as the sum of the Cramér-Rao lower Bound (CRB) of the parameter estimates assuming a perfect knowledge of the transmitted waveform and the excess contribution due to noise in the reference channels.
- 4) A compact expression for the CRB that involves only the parameters of interest (delay and Doppler).
- 5) Based on the above, explicit guidelines for the SNR in the RC in order for the parameter estimates to achieve the mentioned CRB.

Further, it is demonstrated how to extend the estimation method and the analysis to the case of long observation times and/or fast targets, which results in non-negligible variations in the time-delay parameter(s) over the observation interval. The paper is organized as follows:

A. Symbols and notation

We will indicate *column* vectors with bold lowercase letters $\mathbf{a}, \mathbf{b}, \dots$ and matrices with bold uppercase letters $\mathbf{A}, \mathbf{B}, \dots$ The component-wise Hadamard product will be denoted by \odot . The norm $\|\cdot\|$ is the ℓ^2 norm unless otherwise specified.

II. PROBLEM DESCRIPTION

We consider a passive radar scenario, where K receiver nodes collect data emanating from N_I IOs. See Figure 1 for a scenario with one IO and one RC node. The nodes receive both the direct path, collected via the RC, and reflected signals from N_T targets, collected through the SC.

The RC is equipped with a directive antenna, whereas the SC antenna senses the entire area where targets can appear. For simplicity, we assume $N_I = 1$, i.e. only one IO is considered. The extension to $N_I > 1$ is straightforward, provided the individual waveforms from each IO can be extracted separately, as in e.g. [13]. Likewise, we consider only the case $N_T = 1$, although the presented method can be applied to multiple sufficiently well-separated targets by searching for multiple peaks in the global likelihood function to be defined.

The following assumptions are made:

- Each RN is equipped with co-located RC and SC channels. The RC receives the direct IO signal with high SNR and no target or clutter returns.
- The targets of interest are moving at constant non-zero speeds. SC contributions from stationary objects as well as the direct IO signal are considered interference.
- The RNs can transmit data to a Central Node (CN) after appropriate pre-processing. The data from different receiver nodes are synchronized to time-delay (relative bandwidth) but not phase (relative carrier).
- The positions of the IO and the RNs are known at the CN. For simplicity, we consider a 2D geometry with spatial coordinates x and y . The extension to 3D comes with a higher computational demand, but is otherwise straightforward.
- The RC and SC receivers at each node share the same oscillator and thus experience the same phase noise, which is therefore neglected.

III. DATA MODEL

The IO transmits a signal $\Re\{s(t)e^{j\omega_c t}\}$, where $s(t)$ is the baseband complex envelope and ω_c the carrier frequency. Given the description and assumptions in the previous section, the available data after demodulation at node k , $k = 1, \dots, K$, is modeled by

$$x_k(t) = a_k s_k(t) + n_k(t) \quad (1)$$

$$y_k(t) = b_k s_k(t) + s_k^c(t) + d_k s_k(t - \tau_k) e^{j\omega_k t} + e_k(t), \quad (2)$$

where $x_k(t)$ and $y_k(t)$ represent the data from the reference and the surveillance channel respectively. In both equations above, $s_k(t)$ is the delayed IO signal arriving at node k , thus serving as a reference for that node. The delay is known at the CN, since the position of the IO and the nodes are assumed known, and for simplicity we define $t = 0$ as the start of the SC data collection at each node. The RC (1) consists of the direct path, where a_k accounts for propagation attenuation and receiver characteristics, and receiver noise $n_k(t)$. In the SC (2), the first term is the DPI, the second collects clutter from stationary objects, the third is the target reflection, and the last term is receiver noise. The complex target amplitude d_k accounts for propagation attenuation, bi-static Radar Cross Section (RCS) as well as antenna and receiver gain. The factor $e^{j\omega_k t}$ represents the Doppler effect due to the bi-static range rate, as seen from RN k (see below). The target is assumed to move with a constant speed, which is sufficiently low so that the geometry of the bi-static scenario does not change significantly over the data collection interval. From Figure 1 (see also, e.g. [26]), the time-delay of the target signal can be expressed as

$$\tau_k = \frac{\|\mathbf{u} - \mathbf{r}_k\| + \|\mathbf{u} - \mathbf{r}\|}{c} - \frac{\|\mathbf{r}_k - \mathbf{r}\|}{c}, \quad (3)$$

where $\mathbf{u} = (x, y)^T$ is the target position vector, \mathbf{r}_k is the location of the k th RN, \mathbf{r} is the IO position, and c is the speed of propagation. Notice that the line-of-sight delay has been

subtracted in (3) to comply with the model in (2). Denoting $r_k = \|\mathbf{u} - \mathbf{r}_k\|$ and $r = \|\mathbf{u} - \mathbf{r}\|$, the time derivative of τ_k due to a constant velocity $\dot{\mathbf{u}} = (v_x, v_y)^T$ is given by

$$\dot{\tau}_k = \frac{1}{c} \left(\frac{\dot{\mathbf{u}}^T(\mathbf{u} - \mathbf{r}_k)}{r_k} + \frac{\dot{\mathbf{u}}^T(\mathbf{u} - \mathbf{r})}{r} \right). \quad (4)$$

If we let the initial time-delay w.r.t. the reference be $\tau_k(0) = 0$, the time-varying time-delay is simply given by $\tau_k(t) = \dot{\tau}_k t$, and we find that the target Doppler frequency ω_k is related to $\dot{\tau}_k$ by

$$\omega_k = -\dot{\tau}_k \omega_c \quad (5)$$

It is clear that each RN can only determine the time-delay and Doppler of the target as seen from its own position. Given (τ_k, ω_k) pairs from sufficiently many RNs, there is a unique target position and velocity vector that satisfies (3) – (5) for all k . The general problem under consideration herein is to estimate \mathbf{u} and $\dot{\mathbf{u}}$ from measured data at the RC and SC channels at K nodes. We do not specifically address the detection problem, but simply assume knowledge of the presence of precisely one target.

Let the data collection time in the SC be $0 \leq t < T$, in which N samples are collected at time instances $t_n = n\Delta T$, $\Delta T = T/N$, $n = 0, \dots, N-1$. The sampling time ΔT satisfies $\Delta T \leq 1/B$, where B is the bandwidth of $s_k(t)$. If $\dot{\tau}_k$ is much smaller than $\Delta T/T = 1/N$, the time-delay in $s(t - \tau_k(t)) \approx s(t - \tau_k(0))$ is the same for all samples. If this is not the case, so-called *range cell migration* may occur, so that the discrete-time delay (corresponding to bistatic target range gates) is not constant during the data collection interval. See, e.g. [27], [28] for details and mitigation for the mono-static case. To simplify the exposition, we will in the developments that follow assume that the above holds, expressing the time-delayed (baseband) waveform as $s(t - \tau)$, where τ is a constant parameter. An extension to the more general case is provided in Section IV-D below.

The task at each RN is to either estimate its own time-delay and Doppler parameters from the SC data, or to transmit a certain test statistic to the CN. The time-delay and Doppler parameters are related to the target position and velocity as detailed above. Due to the time-delay of the clutter and target components, it is assumed that the data collection starts earlier for the RC. Let the maximum delay of interest be M samples. The available data samples are then $\{x_k(t_n)\}_{n=-M}^{N-1}$ and $\{y_k(t_n)\}_{n=0}^{N-1}$, which can be put into vector form as

$$\mathbf{x}_k^R = a_k \mathbf{s}_k^R + \mathbf{n}_k \quad (6)$$

$$\mathbf{y}_k = b_k \mathbf{s}_k + \mathbf{s}_k^c + d_k \mathbf{s}_k(\tau_k) \odot \mathbf{v}(\omega_k) + \mathbf{e}_k, \quad (7)$$

where $\mathbf{x}_k^R = [x_k(t_{-M}), \dots, x_k(t_{N-1})]^T$ is the observed RC signal vector, \mathbf{s}_k^R is the similarly defined vector of transmitted waveforms, whereas $\mathbf{y}_k = [y_k(t_0), \dots, y_k(t_{N-1})]^T$ and $\mathbf{s}_k(\tau_k) = [s_k(t_0 - \tau_k), \dots, s_k(t_{N-1} - \tau_k)]^T$ are the SC signals, with the simplified notation $\mathbf{s}_k = \mathbf{s}_k(0)$ for the waveform

vector at zero delay. Further, for the target signal, $\mathbf{v}(\omega_k)$ denotes the DFT vector

$$\begin{aligned} \mathbf{v}(\omega_k) &= [e^{j\omega_k t_0}, \dots, e^{j\omega_k t_{N-1}}]^T \\ &= [1, e^{j\omega_k \Delta T}, \dots, e^{j\omega_k (N-1)\Delta T}]^T, \end{aligned} \quad (8)$$

and \odot represents the Schur/Hadamard product (elementwise multiplication). The clutter component is assumed to be well-modeled as a linear combination of a finite set of past samples of the IO signal, i.e. an FIR filter:

$$\mathbf{s}_k^c(t_n) = \sum_{l \in \mathcal{L}_c} c_l s_k(t_n - l\Delta T) = \sum_{l=1}^L c_l s_k(t_n - l\Delta T),$$

where the set \mathcal{L}_c , of cardinality L , $L \leq M$, contains the range of time delays l for which we expect clutter returns. For the sake of simplicity, we assume in the second equality that $\mathcal{L}_c = \{1, \dots, L\}$. Hence, we can express the clutter vector in (7) as

$$\mathbf{s}_k^c = \mathbf{S}_k \mathbf{c}_k, \quad (9)$$

where \mathbf{S}_k is an $N \times L$ Toeplitz matrix containing samples of $s_k(t_n - l\Delta T)$ for $l = 1$ and $n = 0, \dots, N-1$ as its first column, and for $n = 0$ and $l = 1, \dots, L$ as its first row; and where $\mathbf{c}_k = [c_1, \dots, c_L]^T$ is the vector of complex-valued FIR filter coefficients. The noise samples are all assumed to be i.i.d. WGN with variances σ_n^2 and σ_e^2 respectively. Thus, \mathbf{n}_k and \mathbf{e}_k are zero-mean independent Gaussian random vectors with covariance matrices $\sigma_n^2 \mathbf{I}_{M+N}$ and $\sigma_e^2 \mathbf{I}_N$ respectively, where the dimension of the respective identity matrix has been stressed for clarity.

IV. PARAMETER ESTIMATION AND TARGET LOCALIZATION

In this section, we present the ECA approach of [9] as an approximate ML estimator. Target localization is performed at the CN, by combining information from each node. The SC data at each node holds information about the target's time-delay and Doppler, as seen from its own location. However, the target contribution is corrupted by DPI and clutter, which must therefore be canceled at each RN before computing a suitable “test statistic” to be transmitted to the CN. In effect, this is achieved by using the RC data as replacement of the unknown transmitted waveform.

A. Interference Cancellation and Delay-Doppler Estimation

Under the above assumptions and modeling the IO signal vector \mathbf{s}_k as deterministic and unknown [10], [11], [29], the global Maximum Likelihood (ML) approach leads to a combination of likelihood functions from each node. At node k , the negative log-likelihood function, ignoring constants, is given by

$$\frac{1}{\sigma_n^2} \|\mathbf{x}_k^R - a_k \mathbf{s}_k^R\|^2 + \frac{1}{\sigma_e^2} \|\mathbf{y}_k - \mathbf{S}_{I,k} \mathbf{f}_k - d_k \mathbf{s}_k(\tau_k) \odot \mathbf{v}(\omega_k)\|^2, \quad (10)$$

where we have collected the interference contribution to the SC in the matrix $\mathbf{S}_{I,k} = [\mathbf{s}_k \mathbf{S}_k]$, with amplitude vector $\mathbf{f}_k = [b_k \mathbf{c}^T]^T$. The ML estimate is now found by minimizing (10)

with respect to all unknown parameters. Both the RC and the SC contain information about the unknown IO signal, through the first and second terms in (10) respectively. However, since the SNR of the IO signal is much stronger in the RC than in the SC, it is a good approximation to determine the IO signal using the RC data only [10]. This will also significantly simplify the estimation, since the first term in (10) can be put to zero, for example, by absorbing the amplitude into the estimate of \mathbf{s}_k^R and taking $\hat{\mathbf{s}}_k^R = \mathbf{x}_k^R$. Thus, the signal from the reference channel will replace the unknown IO signal when processing the data from the surveillance channel.

Let us denote the estimated IO signal part in the second term of (10) as

$$\hat{\mathbf{S}}_{I,k} = [\hat{\mathbf{s}}_k \hat{\mathbf{S}}_k] = [\mathbf{x}_k \mathbf{X}_k] = \mathbf{X}_{I,k}$$

and $\hat{\mathbf{s}}_k(\tau_k) = \mathbf{x}_k(\tau_k)$, respectively, where the sampling instances in \mathbf{x}_k and \mathbf{X}_k are aligned with those in \mathbf{s}_k and \mathbf{S}_k . Inserted into (10), this yields

$$\ell(\mathbf{f}_k, d_k, \tau_k, \omega_k) = \|\mathbf{y}_k - \mathbf{X}_{I,k}\mathbf{f}_k - d_k \mathbf{x}_k(\tau_k) \odot \mathbf{v}(\omega_k)\|^2. \quad (11)$$

Note that both τ_k and ω_k are known functions of the target position and velocity vector, see (3)–(5). The latter are collected in the parameter vector $\boldsymbol{\theta} \in \mathbb{R}^4$ to be defined in Section IV-B. Also note that since $\mathbf{x}_k \approx a_k \mathbf{s}_k$ contains the RC signal amplitude, the estimated amplitude parameters b_k , \mathbf{c}_k and d_k will in effect be normalized with respect to a_k .

Minimizing (11) w.r.t. \mathbf{f}_k and substituting the resulting estimate back into (11), results in an effective cancellation of the direct IO and the clutter interference. The orthogonal projection matrices onto the orthogonal complements of the span of $\mathbf{S}_{I,k}$ and $\mathbf{X}_{I,k}$ are given, respectively, by

$$\boldsymbol{\Pi}^\perp = \mathbf{I} - \boldsymbol{\Pi} = \mathbf{I} - \mathbf{S}_{I,k} \left(\mathbf{S}_{I,k}^H \mathbf{S}_{I,k} \right)^{-1} \mathbf{S}_{I,k}^H \quad (12)$$

$$\hat{\boldsymbol{\Pi}}^\perp = \mathbf{I} - \hat{\boldsymbol{\Pi}} = \mathbf{I} - \mathbf{X}_{I,k} \left(\mathbf{X}_{I,k}^H \mathbf{X}_{I,k} \right)^{-1} \mathbf{X}_{I,k}^H. \quad (13)$$

Note that we will frequently drop the index k in the various quantities, since it can be understood from the context. Also note that the amplitude scaling in $\mathbf{X}_{I,k}$ has no effect on the projection matrix, so in the absence of noise we have $\hat{\boldsymbol{\Pi}} = \boldsymbol{\Pi}$.

With these definitions, the minimum of (11) w.r.t. \mathbf{f}_k reduces to the interference-cleaned criterion function

$$\ell(d_k, \tau_k, \omega_k) = \left\| \hat{\boldsymbol{\Pi}}^\perp \{ \mathbf{y}_k - d_k \mathbf{x}_k(\tau_k) \odot \mathbf{v}(\omega_k) \} \right\|^2. \quad (14)$$

Next, we introduce the delay-Doppler “steering vector” $\mathbf{a}(\tau_k, \omega_k)$, along with its estimate $\hat{\mathbf{a}}(\tau_k, \omega_k)$, obtained from the RC data as

$$\mathbf{a}(\tau_k, \omega_k) = \mathbf{s}_k(\tau_k) \odot \mathbf{v}(\omega_k) \quad (15)$$

$$\hat{\mathbf{a}}(\tau_k, \omega_k) = \mathbf{x}_k(\tau_k) \odot \mathbf{v}(\omega_k). \quad (16)$$

We remind that the amplitude a_k is present in (16) but not in (15). Substituting the minimizing d_k from (14) back into the criterion then results in the final form

$$\ell(\tau_k, \omega_k) = \left\| \hat{\boldsymbol{\Pi}}^\perp \mathbf{y}_k - \hat{\boldsymbol{\Pi}}^\perp \frac{\hat{\mathbf{a}}(\tau_k, \omega_k) \hat{\mathbf{a}}^H(\tau_k, \omega_k)}{\hat{\mathbf{a}}^H(\tau_k, \omega_k) \hat{\boldsymbol{\Pi}}^\perp \hat{\mathbf{a}}(\tau_k, \omega_k)} \hat{\boldsymbol{\Pi}}^\perp \mathbf{y}_k \right\|. \quad (17)$$

Clearly, minimizing $\ell(\tau_k, \omega_k)$ is equivalent to maximizing the following interference-canceled and normalized version of the cross ambiguity function, or “spectrum”:

$$P_k(\tau_k, \omega_k) = \frac{|\hat{\mathbf{a}}^H(\tau_k, \omega_k) \hat{\boldsymbol{\Pi}}^\perp \mathbf{y}_k|^2}{\hat{\mathbf{a}}^H(\tau_k, \omega_k) \hat{\boldsymbol{\Pi}}^\perp \hat{\mathbf{a}}(\tau_k, \omega_k)} = \left\| \hat{\mathbf{P}} \mathbf{y}_k \right\|^2, \quad (18)$$

where $\hat{\mathbf{P}}$ is the orthogonal projection matrix onto the range space of $\hat{\boldsymbol{\Pi}}^\perp \hat{\mathbf{a}}(\tau_k, \omega_k)$:

$$\hat{\mathbf{P}} = \frac{\hat{\boldsymbol{\Pi}}^\perp \hat{\mathbf{a}}(\tau_k, \omega_k) \hat{\mathbf{a}}^H(\tau_k, \omega_k) \hat{\boldsymbol{\Pi}}^\perp}{\hat{\mathbf{a}}^H(\tau_k, \omega_k) \hat{\boldsymbol{\Pi}}^\perp \hat{\mathbf{a}}(\tau_k, \omega_k)} = \mathbf{I} - \hat{\mathbf{P}}^\perp. \quad (19)$$

Although (18) depends implicitly on the target position and speed vector, the k -th receiver node can only evaluate the criterion with respect to the target delay and Doppler parameters relative its own position. Thus, ideally, at node k , (18) is computed on a (τ_k, ω_k) -grid, and the “significant” values are transmitted to the central node for further processing.

B. Target Localization

The final step is to combine the delay-Doppler information from all receiver nodes using a global Maximum Likelihood approach at the central node. In principle, this can be done using local estimates at each RN, such as in classical source localization. See, e.g., [30] for methods based on time-delays only and [26], [31] for localization using time-delay and Doppler. However, such an approach, albeit being more convenient from a communication point of view, is inherently suboptimal from a statistical performance perspective. Thus, we assume the available data to be (the sampled versions of) (18) from all nodes. Since the data are independent, the global likelihood function simply adds all contributions with appropriate weightings:

$$V(\boldsymbol{\theta}) = \sum_{k=1}^K w_k P_k(\tau_k(\boldsymbol{\theta}), \omega_k(\boldsymbol{\theta})), \quad (20)$$

where $\tau_k = \tau_k(\boldsymbol{\theta})$ and $\omega_k = \omega_k(\boldsymbol{\theta})$ are functions of the target parameter vector $\boldsymbol{\theta} = [x, y, v_x, v_y]^T$, as given by (3)–(5). The weights w_k should be chosen as the inverse of the SC noise variance at each RN. For simplicity, we take $w_k \equiv 1$ in the following. The global ML estimator is now to perform a global search for maximizing (20) w.r.t. the 4-dimensional target parameter vector $\boldsymbol{\theta}$. For each hypothesized target localization and velocity, the corresponding time-delay and Doppler parameters are calculated for each node. The resulting value of (18) is added to the global likelihood function, and if this sample is missing at a particular node we simply add zero. This is clearly a computationally very demanding task, and there is a need for simpler, suboptimal, methods to find good initial values for a gradient-type search. This is beyond the scope of the present paper; our main goal being to quantify the achievable performance with such an optimal approach.

C. Frame-Based Processing

The available data set can be quite large, which makes it more practical to process data in frames, similar to [9]. The data can then be divided into M batches, each of size $Q = N/M$. The model (6)–(7) is then applied to each such batch. Thus, at the k :th RN, we simply write for the m :th batch

$$\mathbf{x}_{k,m}^R = a_{k,m} \mathbf{s}_{k,m}^R + \mathbf{n}_{k,m} \quad (21)$$

$$\mathbf{y}_{k,m} = \mathbf{S}_{I,k,m} \mathbf{f}_{k,m} + d_{k,m} \mathbf{a}_{k,m}(\tau_k, \omega_k) + \mathbf{e}_{k,m}, \quad (22)$$

where $\mathbf{a}_{k,m}(\tau_k, \omega_k) = \mathbf{s}_{k,m}(\tau_k) \odot \mathbf{v}(\omega_k)$, for $m = 1, \dots, M$. The simplification now comes from computing the interference-cleaned cross ambiguity function for each batch separately, and adding them incoherently. Clearly, this reduces the memory requirements and allows for parallel processing.

The most straightforward way to implement the frame-based processing is to arrange the data into consecutive batches, so that the m :th data vector $\mathbf{y}_{k,m}$ contains data samples $\{y(t_n)\}$ for $n = \{(m-1)Q, (m-1)Q+1, \dots, mQ-1\}$ and $m = 1, \dots, M$. Clearly, this reduces the resolution in both time-delay and Doppler, since the length of each batch is reduced by a factor of M . An alternative that preserves most of the resolution is to instead choose $\mathbf{y}_{k,m}$ to contain every M :th sample of \mathbf{y}_k , i.e. samples $\{y(t_n)\}$ for $n = \{m-1, m-1+M, \dots, m-1+M(Q-1)\}$ and $m = 1, \dots, M$. Since this effectively implies a down-sampling of the signal, the price to pay is that the non-ambiguous Doppler shift is reduced. Specifically, this “sparse sampling” approach requires $|\omega_k| < \pi/M$, which puts a limit to the number of batches that can be used. Provided this condition is met, we expect the sparse sampling approach to frame-based processing to yield superior performance as compared to the version with consecutive samples.

In the model (22), the DFT vector $\mathbf{v}(\omega_k)$, similar to (8) but of length Q , is the same for all k and m . This is because we let the extra phase shift for increasing m be captured by the complex amplitude $d_{k,m}$, i.e. non-coherent combination. Note that the same $\mathbf{v}(\omega_k)$ is used for both sampling strategies, but for the sparse sampling approach the Doppler parameter needs to be scaled by M to fit the original sampling time.

Given the model (22), the interference-cleaned cross ambiguity function is computed as in Section IV-A. Stressing the indices k, m to indicate node k and batch m , we have

$$P_{k,m}(\tau_k, \omega_k) = \frac{|\hat{\mathbf{a}}_{k,m}^H(\tau_k, \omega_k) \hat{\mathbf{\Pi}}_{k,m}^\perp \mathbf{y}_{k,m}|^2}{\hat{\mathbf{a}}_{k,m}^H(\tau_k, \omega_k) \hat{\mathbf{\Pi}}_{k,m}^\perp \hat{\mathbf{a}}_{k,m}(\tau_k, \omega_k)}$$

These batch-wise spectra can now be added incoherently to form the total frame-based spectrum estimate:

$$P_k(\tau_k, \omega_k) = \sum_{m=1}^M P_{k,m}(\tau_k, \omega_k). \quad (23)$$

It is noted here that the frame-based division of data is only used for the interference cancellation in [9]. The cross-ambiguity function is then computed using all batches together, as in (18), where $\hat{\mathbf{\Pi}}^\perp$ is now a block-diagonal matrix.

This will therefore avoid the loss of resolution of target parameters, similarly to the sparse sampling approach. For comparison purposes, we still use the in-coherent combination (23), which enables a simple extension of the statistical analysis to be presented.

As before, the aggregated functions $P_k(\tau_k, \omega_k)$ are input to (20), to perform the target localization using data from all RN:s. Since the IC is done independently in each batch, ignoring the fact that the estimated interference parameters should all be the same, the batch-mode processing comes with a price in the form of reduced statistical performance. The gain is mainly in the need for memory and also the fact that the spectrum can be computed in parallel for each batch.

D. Including Range Migration

In the above development it has been assumed that the time-delay, τ_k , of the received signal waveform remains the same throughout the data collection interval. Taking the linear time-variation of the time-delay (4) into account, $\tau_k(t)$ becomes coupled to the Doppler parameter ω_k through the relation (5), which is expressed as

$$\tau_k(t) = \tau_k(0) - \frac{\omega_k}{\omega_c} t = \tau_k - \frac{\omega_k}{\omega_c} t, \quad (24)$$

where, with some abuse of notation, we still let $\tau_k = \tau_k(0)$ denote the initial time-delay parameter. Rather than compensating the data for the range migration effect, as in [27], [28], we propose to incorporate the relation (24) into the signal model. Thus, the delay-Doppler steering vector definitions (15) – (16) are modified as

$$\mathbf{a}(\tau_k, \omega_k) = \mathbf{s}_k(\tau_k, \omega_k) \odot \mathbf{v}(\omega_k) \quad (25)$$

$$\hat{\mathbf{a}}(\tau_k, \omega_k) = \mathbf{x}_k(\tau_k, \omega_k) \odot \mathbf{v}(\omega_k), \quad (26)$$

where the n :th components of $\mathbf{s}_k(\tau_k, \omega_k)$ and $\mathbf{x}_k(\tau_k, \omega_k)$ are, respectively, given by $s(t_n - \tau_k + \frac{\omega_k}{\omega_c} t_n)$ and $x(t_n - \tau_k + \frac{\omega_k}{\omega_c} t_n)$, $n = 0, \dots, N-1$.

With this modification, the spectrum $P_k(\tau_k, \omega_k)$ can still be computed according to the formula (18). In fact, also the performance analysis to follow remains unchanged with the above modifications. We remark that the estimator and the analysis can, with some effort, be adapted also to the case where the target motion causes a non-negligible effect to the geometry, so that $\dot{\tau}_k$ is not constant over the data collection time.

V. PERFORMANCE ANALYSIS

The proposed global ML estimator is approximate in the sense that it uses the reference channel as if it were the true IO signal. It is of interest to quantify analytically the effect of this approximation. Specifically, what SNR is required in the reference channel in order for the approximate ML estimates to achieve the Cramér-Rao lower bound for the target parameters, assuming a perfect IO signal knowledge?

A. Consistency

The first step is to establish consistency, in the sense that for noise-free data, the criterion function (18) is maximized by the true target delay-Doppler pair, as seen from the k :th RN. It is easy to establish this result if the IO signal is such that the steering vector is *unambiguous*. By this we mean that the following holds true over the range of target parameters of interest:

$$\text{rank} \left[\mathbf{a}(\tau_0, \omega_0) \mathbf{a}(\tau, \omega) \right] = 1 \iff (\tau_0, \omega_0) = (\tau, \omega), \quad (27)$$

for all $\tau, \tau_0 \in \mathbb{R}$ and $\omega, \omega_0 \in (-\pi/\Delta T, \pi/\Delta T]$. As before, the steering vector is defined by $\mathbf{a}(\tau, \omega) = \mathbf{s}(\tau) \odot \mathbf{v}(\omega)$. That the condition in (27) implies statistical consistency of the estimator can be proved as follows: when the noise variances $\sigma_n^2 \rightarrow 0$ and $\sigma_e^2 \rightarrow 0$ vanish simultaneously, the criterion (11) converges in the mean-square sense to its noise-free version

$$\ell_0(\boldsymbol{\eta}) = \|\mathbf{S}_I \mathbf{f}_0 + d_0 \mathbf{a}(\tau_0, \omega_0) - \mathbf{S}_I \mathbf{f} - d \mathbf{a}(\tau, \omega)\|^2, \quad (28)$$

where $\boldsymbol{\eta} = \{\mathbf{f}, d, \tau, \omega\}$ represents the set of unknown parameters, $\boldsymbol{\eta}_0$ its “true” value, and where we have replaced $\mathbf{x}(\tau)$ and \mathbf{X}_I by the noise-free versions $\mathbf{s}(\tau)$ and \mathbf{S}_I , since the amplitude is irrelevant here. Provided the convergence is uniform in $\boldsymbol{\eta}$, which is true if $\mathbf{s}(\tau)$ has bounded derivatives, then $\hat{\boldsymbol{\eta}}$ converges in the mean-square sense to the minimizer of (28). Clearly, $\ell_0(\boldsymbol{\eta}) \geq 0$, with equality if and only if

$$\left[\mathbf{S}_I \quad \mathbf{a}(\tau_0, \omega_0) \quad \mathbf{a}(\tau, \omega) \right] \begin{bmatrix} \mathbf{f}_0 - \mathbf{f} \\ d_0 \\ -d \end{bmatrix} = 0. \quad (29)$$

Provided the target is present so that $|d_0| > 0$, the above is possible only if $\tau = \tau_0$ and $\omega = \omega_0$, if (27) holds and if the vector $\mathbf{a}(\tau_0, \omega_0)$ is not in the span of \mathbf{S}_I . It also follows from (27) that the latter is satisfied whenever the target has non-zero Doppler, $\omega_0 \neq 0$. Further, if \mathbf{S}_I is full rank, it also follows that $\mathbf{f} = \mathbf{f}_0$, i.e. $b = b_0$ and $\mathbf{c} = \mathbf{c}_0$. In principle, it is also possible to localize a stationary target, provided it is known to reside outside the clutter-contaminated range bins. But since we are more interested in the case where the target is obscured by clutter, we consider only the case $\omega_0 \neq 0$.

The following Theorem 1 clarifies that (27) is satisfied for a certain class of stochastic processes. The proof is deferred to Appendix C.

Theorem 1. *Let $s(t)$ be a circularly symmetric complex-valued bandlimited wide-sense stationary Gaussian stochastic process, with zero mean and spectral density $\mathcal{S}_s(f) = 1$ supported in $[-B/2, B/2]$, with $B > 0$. Let $0 \leq t_1 < t_2 < \dots < t_N$, $N \geq 3$, be some fixed real sampling times, and τ_0, ω_0 some fixed real parameters. Define the random vector*

$$\mathbf{v} = (s(t_1 - \tau_0)e^{i\omega_0 t_1}, \dots, s(t_N - \tau_0)e^{i\omega_0 t_N})^T$$

and the random field

$$\mathbf{w}(\tau, \omega) = (s(t_1 - \tau)e^{i\omega t_1}, \dots, s(t_N - \tau)e^{i\omega t_N})^T.$$

Then, \mathbf{v} and $\mathbf{w}(\tau, \omega)$ are linearly independent w.p.1:

$$\text{Prob} \left(\exists (\tau, \omega) \in T : \text{rank} (\mathbf{v} \quad \mathbf{w}(\tau, \omega)) = 1 \right) = 0, \quad (30)$$

where T can be chosen to be the cartesian product between a finite union of disjoint nonempty bounded closed intervals, not containing τ_0 , and \mathbb{R} .

In what follows, we will assume (27) to be true so that the time-delay and Doppler parameters can be uniquely determined at each RN. It is also assumed that the geometry of the scenario is such that $\boldsymbol{\theta}$ can be uniquely retrieved from the $\{(\tau_k, \omega_k)\}_{k=1}^K$ pairs. This is obviously true for a “large enough” number of RNs, placed, say, in a random fashion. A precise statement regarding the requirement appears to be an open problem, but a complete solution was recently provided for the related GPS problem [32].

B. Asymptotic Covariance Matrix

The global ML estimate of the target parameters is obtained by maximizing (20) w.r.t. $\boldsymbol{\theta}$. Thus, treating $\boldsymbol{\theta}$ as a continuous-valued parameter, the gradient is zero at the optimal value,

$$V'(\hat{\boldsymbol{\theta}}) = 0, \quad (31)$$

where $\hat{\boldsymbol{\theta}}$ denotes the ML estimate. Assuming a large number of samples or high SNR, $\hat{\boldsymbol{\theta}}$ will be close to the true value, say $\boldsymbol{\theta}_0$. Then, a standard first-order expansion of (31) gives the first-order expression for the estimation error

$$\hat{\boldsymbol{\theta}} - \boldsymbol{\theta}_0 \simeq -\mathbf{H}^{-1} V'(\boldsymbol{\theta}_0), \quad (32)$$

where \mathbf{H} is the limiting Hessian matrix as either $N \rightarrow \infty$ (assuming the limit to exist) or $\sigma_n^2, \sigma_e^2 \rightarrow 0$. From this expression we can compute the asymptotic covariance matrix of the estimation error as

$$\mathbb{E}[(\hat{\boldsymbol{\theta}} - \boldsymbol{\theta}_0)(\hat{\boldsymbol{\theta}} - \boldsymbol{\theta}_0)^T] \approx \mathbf{H}^{-1} \mathbb{E}[V'(\boldsymbol{\theta}_0)V'^T(\boldsymbol{\theta}_0)] \mathbf{H}^{-1}. \quad (33)$$

Since we do not make any assumptions on the transmitted waveform, only the case of “sufficiently high” SNR is considered, i.e. σ_n^2, σ_e^2 being small enough. In the following, we provide compact expressions for the Hessian matrix and the first-order approximation (in σ_n^2 and σ_e^2) of the covariance matrix of the gradient appearing in (33).

In order to express the approximate covariance matrix in a compact form, the following notation is first introduced. Let

$$\mathbf{D}_k = \left[\frac{\partial \mathbf{a}(\tau_k(\boldsymbol{\theta}), \omega_k(\boldsymbol{\theta}))}{\partial \theta_1}, \dots, \frac{\partial \mathbf{a}(\tau_k(\boldsymbol{\theta}), \omega_k(\boldsymbol{\theta}))}{\partial \theta_4} \right] \quad (34)$$

denote the Jacobian matrix of the k :th steering vector. We note, in passing, that the analysis presented in the following is also applicable to the estimation of τ_k and ω_k at a single node, simply by using $\boldsymbol{\theta} = [\tau_k, \omega_k]^T$ in (34) and not performing the sum over k . Further, define the $N \times N(L+1)$ matrix

$$\mathbf{Z}_k = [b_k \mathbf{I} + d_k \text{diag}(\mathbf{v}(\omega_k)) \quad \mathbf{c}_k^T \otimes \mathbf{I}], \quad (35)$$

and let \mathbf{J}_k be a selection matrix such that

$$\text{vec}(\mathbf{S}_I) = \mathbf{J}_k \mathbf{s}_I,$$

where $\mathbf{s}_I = [s_k(t_{-L}), \dots, s_k(t_{N-1})]^T$. The three components in (35) model the error contributions to $\hat{\boldsymbol{\theta}}$ due to not knowing the IO waveform perfectly. The first term to the left is due to

imperfect DPI cancellation and the second handles the effect of using the incorrect steering vector in (18), i.e. a “mismatched filter”. The right component comes from the imperfect clutter cancellation.

Further, let \mathbf{P} be the noise-free version of $\tilde{\mathbf{P}}$, defined in (19), and introduce the orthogonal projection matrix

$$\tilde{\mathbf{P}} = \mathbf{\Pi}^\perp \mathbf{P}^\perp \mathbf{\Pi}^\perp, \quad (36)$$

which projects onto $\text{span}(\mathbf{\Pi}^\perp \mathbf{B})$, where \mathbf{B} is any matrix that spans the orthogonal complement of the steering vector \mathbf{a} . We can now state the main result of this paper.

Theorem 2. *Let $\hat{\theta}$ be obtained by maximizing (20) and assume the IO waveform be such that (27) holds. Assume further that the radar scenario is such that the $\{(\tau_k, \omega_k)\}_{k=1}^K$ pairs together uniquely determine θ . Then, as $\sigma_n^2 \rightarrow 0$ and $\sigma_e^2 \rightarrow 0$ jointly, we have $\hat{\theta} \rightarrow \theta_0$ in probability; and its covariance matrix is to first order given by*

$$\mathbb{E}[(\hat{\theta} - \theta_0)(\hat{\theta} - \theta_0)^T] \approx \mathbf{CRB}_\theta + \mathbf{H}^{-1} \mathbf{Q} \mathbf{H}^{-1}, \quad (37)$$

where

$$\mathbf{CRB}_\theta = \sigma_e^2 \mathbf{H}^{-1} = \frac{\sigma_e^2}{2} \left(\sum_{k=1}^K |d_k|^2 \Re \{ \mathbf{D}_k^H \tilde{\mathbf{P}} \mathbf{D}_k \} \right)^{-1} \quad (38)$$

$$\mathbf{Q} = 2\sigma_n^2 \sum_{k=1}^K \frac{|d_k|^2}{|a_k|^2} \Re \{ \mathbf{D}_k^H \tilde{\mathbf{P}} \mathbf{Z}_k \mathbf{J}_k \mathbf{J}_k^T \mathbf{Z}_k^H \tilde{\mathbf{P}} \mathbf{D}_k \}. \quad (39)$$

The term \mathbf{CRB}_θ in (37) is the CRLB for θ assuming a perfectly known IO signal, and the second term quantifies the excess error due to the noise in the reference channel.

Proof. The covariance matrix of the gradient and the asymptotic Hessian matrix are derived, respectively, in Appendices A and B. Putting these together according to (33) leads to (37). \square

Remark 1 The fact that (38) is the CRB for θ assuming a perfect reference signal follows from the fact that when $\sigma_n^2 = 0$, $\hat{\theta}$ is the exact ML estimate of θ , which is statistically efficient to first order under mild conditions [33]. To be precise, (38) is the CRB only if it is computed with $M = 1$. For $M > 1$, one could in principle define a CRB for frame-based data, which would then be valid under the assumption that the frames are not synchronized. \square

C. Statistical Efficiency

Using the results from the previous section, we can now address the question of how large the errors in the reference signal can be in order for its effect to be negligible. We note in passing that while the errors are assumed to emanate from a noisy reference channel, the analysis is useful also if it is due to other effects, such as phase noise, as long as they can be modeled as additive and white.

The expression (37) has two terms, corresponding to the contributions to the estimation error from the noise in the

surveillance channel (first term) and the reference channel (second term), respectively. Thus, the question is how big the second term in (37) is compared to the CRB term. Upon comparing (38)–(39), we can conclude that the matrix $\mathbf{Z}_k \mathbf{J}_k \mathbf{J}_k^T \mathbf{Z}_k^H$ plays a crucial role. Specifically, the second term is negligible if it holds that

$$\|\mathbf{Z}_k \mathbf{J}_k\|_2^2 \ll \frac{\sigma_e^2}{\sigma_n^2} |a_k|^2.$$

We can bound the left hand side using (35) as

$$\begin{aligned} \|\mathbf{Z}_k \mathbf{J}_k\|_2^2 &\leq \|\mathbf{J}_k\|_2^2 \|\mathbf{Z}_k\|_2^2 \leq (L+1) \times \\ &\times \left(\left\| (\mathbf{c}_k^T \otimes \mathbf{I}) \right\|_2^2 + \|b_k \mathbf{I} + d_k \text{diag}(\mathbf{v}(\omega_k))\|_2^2 \right), \end{aligned}$$

where we have used that $\|\mathbf{J}_k\|_2^2 = L+1$, which is easily verified since \mathbf{J}_k is a selection matrix with orthogonal columns and the maximum diagonal element of $\mathbf{J}_k^T \mathbf{J}_k$ is $L+1$. Thus, we conclude that the proposed algorithm will achieve the CRB using a perfectly known reference signal if the following condition is met for all k :

$$(L+1) \frac{|b_k|^2 + |d_k|^2 + \|\mathbf{c}_k\|^2}{\sigma_e^2} \ll \frac{|a_k|^2}{\sigma_n^2}. \quad (40)$$

The right-hand side of (40) is the SNR in the RC, and the left-hand side is an upper bound on the total interference-to-noise ratio in the SC. We recall that the second term in the left-hand side is due to noise in the steering vector (16) when used in (18). Thus, its effect is proportional to the target power, which may seem counterintuitive. We note that the above bound guarantees that the parameter estimates achieve the CRB for a known transmitted signal for *all* values of the target parameters, including targets moving at a very slow speed. For faster targets, there is an additional suppression of the clutter due to the matched-filtering, which may lead to a looser requirement than (40).

VI. NUMERICAL EXAMPLES

In this section we test and validate the theory developed so far with extensive numerical simulations.

A. Baseline validation: single bi-static pair

The first set of numerical experiments consists of Monte Carlo simulations to validate the formula (37) in a bi-static setup, similar to [34].

We set $K = 1$, thus using only $\theta = (\tau, \omega)$ as target parameters. Notice that in this setup the derivative matrix (34) has only two columns: $\partial \mathbf{a} / \partial \tau$ and $\partial \mathbf{a} / \partial \omega$. The baseband IO sensing waveform is chosen to be random and bandlimited with 16 MHz bandwidth and unitary variance; this is subsequently upconverted to Radio Frequency (RF) using a carrier of 600 MHz. The wave is assumed to propagate in space along straight lines, and the amplitudes a_1, b_1 and d_1 are determined using the (deterministic) bi-static radar equation. A single target is present, with radar cross-section $\approx 0.02 \text{ m}^2$, and moving at constant speed of $\approx 200 \text{ m/s}$ (with constant velocity vector $(70, -190) \text{ m/s}$ and corresponding to $\approx 1320 \text{ rad/sec}$ in our bistatic setup). The acquisition time equals $N = 2^{13}$

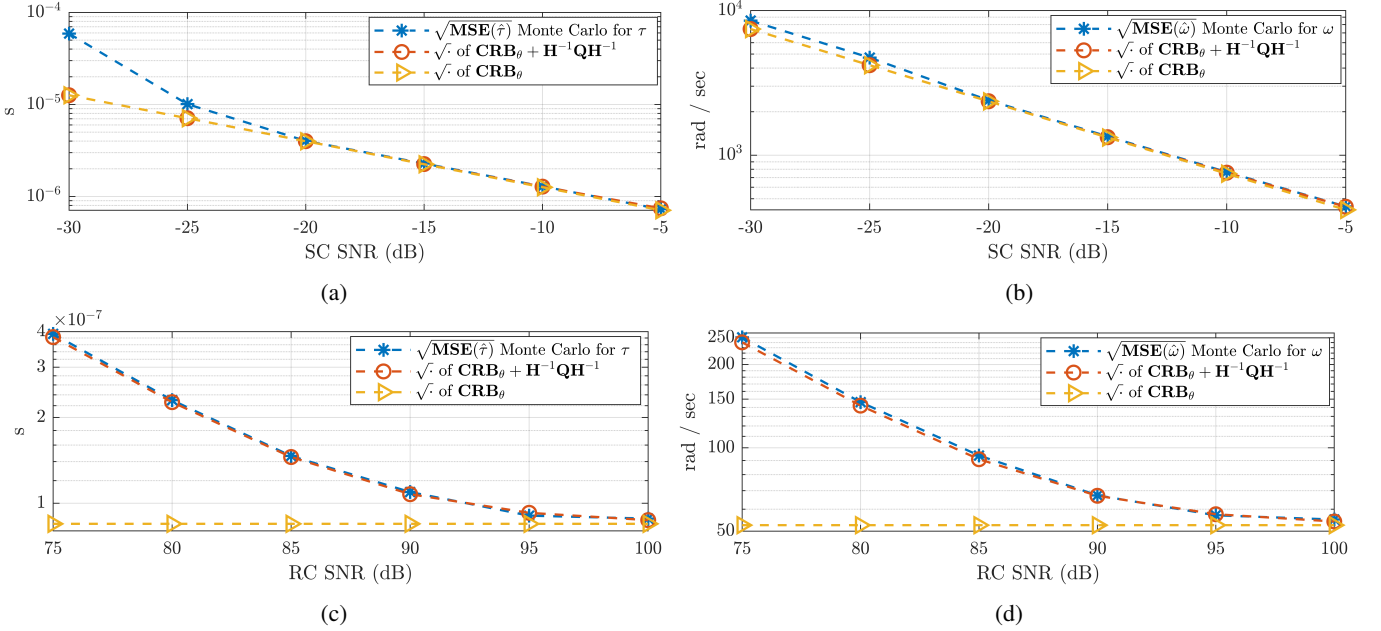


Fig. 2: Empirical and theoretical MSE for estimating time-delay (left plots) and Doppler frequency (right plots) versus SC SNR (top) and RC SNR (bottom) respectively. The RC SNR was kept constant to 75 dB in (2a)-(2b) while the SC SNR was kept constant to 15 dB in (2c)-(2d).

samples, corresponding to approximately 0.33 ms of data at the sampling rate $F_s = 1/\Delta T = 25$ MHz. In Figure 2, we present the results for two scenarios, using different RC and SC SNR levels respectively. The empirical MSE (Mean-Square-Error) values are based on 3000 noise instances, and in each the criterion function (20) is maximized using the Nelder-Mead algorithm with the “true” parameter values θ_0 as starting point. Figure 2 summarizes the numerical simulations as described here. It can be seen that the theory agrees well with the empirical results above a certain threshold SC SNR, which in this case is -25 dB for the time-delay estimate. Noteworthy are Figures 2c and 2d, where the excess error caused by noise in the RC is clearly visible. The mismatch between the latter and the CRB is correctly “predicted” by the covariance (37), and it becomes negligible as soon as the condition (40) is satisfied. Note that the requirement on the RC SNR for this to happen is very strict (≥ 95 dB) in this scenario.

B. Batch processing

In this subsection, we again consider a single bi-static pair with the same radar scene as in subsection VI-A, but with the differences that *i*) the SNR is kept fixed in both channels and *ii*) the target moves at a slower speed of 25 m/s (with velocity vector $\approx (14, -20)$ m/s), so the range migration phenomenon is avoided within the full acquisition period. We test the estimator performances when dividing the whole dataset into batches as described in Section IV-C. We fix the single batch size to $Q = 2^{13}$ samples, progressively increasing the number of batches up to $M = 32$. Note that this implies that the total data size (N) is increased with M . RMSE performances are

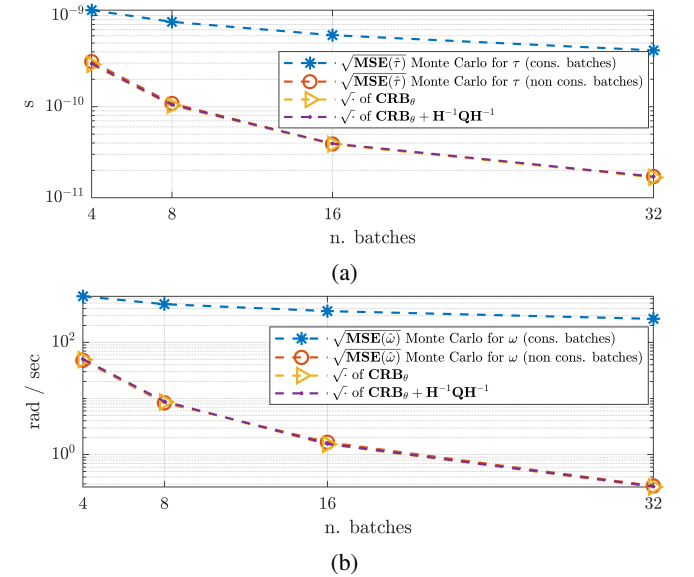


Fig. 3: Empirical and theoretical RMSE of τ (a) and ω (b) for consecutive and non-consecutive batches respectively.

shown in Figure 4, from which it emerges that the consecutive sampling comes with a severe loss in performance, whereas the “sparse sampling” approach approximately attains the CRB at least up to $M = 32$ batches. Thus, using this approach, a very large dataset can be processed in parallel without any notable loss in performance.

C. Target localization: complete multi-static setup

The next step is to validate the formulas (38) and (39) in a multi-node setup. The main difference with the single bi-static setup lies in a dramatic ambiguity reduction, that makes it meaningful to estimate the full suite of parameters $\theta = (x, y, v_x, v_y)^T$. We remind that in the bi-static geometry, the relations between (τ, ω) and (x, y, v_x, v_y) are given by (3) and (4). With this in mind, we perform target localization and velocity estimation using a similar radar scene as in the previous subsections, but with $K = 3$ RNs, located at $(-300, 300)$, $(300, 300)$ and $(-300, -300)$ meters respectively, while the IO sits at $(0, 0)$, and the target moves with motion equation $(10, 10) + (100\sqrt{2}, 100\sqrt{2})t$, $t \geq 0$. Since we assumed constant (thermal) noise power at each RN, the SNR was changed by increasing the transmitter output. This has the effect of changing the SNR in both the SC and the RC, which is why the MSE is approaching the CRB for increasing SNR.

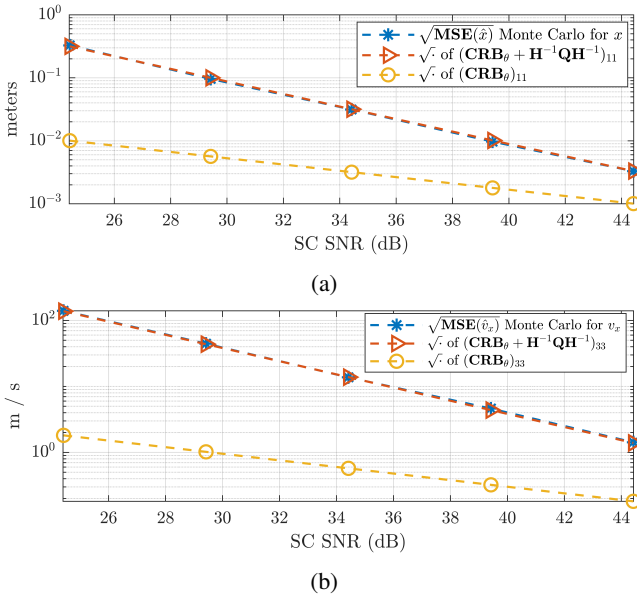


Fig. 4: Monte-Carlo simulation versus theory for localization with 3 RNs. Plots for y and v_y are qualitatively identical and thus omitted. SC SNR is an average over the different RNs.

Figure 4b shows again an excellent agreement between the empirical and the theoretical RMS values. It is also confirmed once more that a very high RC SNR is required to reach the CRB, which assumes a perfect reference signal.

D. Target tracking: complete multi-static setup

To conclude the numerical simulations, we illustrate in Figure 5 an example of "target tracking scenario", where position and velocity estimation is performed within a multi-static setup. No post-filtering is done on the estimates, though. In this scenario, we have 5 RNs located at points $(300 \cos(\alpha_k), 300 \sin(\alpha_k))$ meters with $\alpha_k = 2\pi(k-1)/5$, $k = 1, \dots, 5$. The IO is still located at the origin. We run 5 Monte Carlo noise realizations per sensing interval, and plot

them altogether along with 95% confidence ellipses using (37). The size of the ellipses change as a result of the scenario geometry, as well as the target's acceleration, which is non-zero in this example.

VII. CONCLUSIONS

We have presented a rather complete statistical characterization of the celebrated Extensive Cancelation Algorithm (ECA), due to [9]. The ECA is a method for target localization using several spatially separated passive radar receivers. Each receiver is equipped with a reference channel, with a line-of-sight connection with the illuminator of opportunity, and a surveillance channel that captures reflections from the target(s) of interest. The ECA algorithm uses data from the reference channel to cancel interference in the surveillance channel, in the form of direct-path interference and clutter from stationary objects. After canceling the interference, the time-delay and Doppler parameters are estimated using a non-linear least-squares approach that results in a 2-D spectrum (or cross-ambiguity function). A central node collects information from all receiving stations, and calculates the final target position and velocity estimates. Two extensions of the method are also addressed, namely frame-based processing and range migration. The former means that the data is divided into smaller batches that are analyzed separately, and the latter is the result of rapidly moving targets and/or very long data collection times. The time-delay of the baseband waveform will then vary significantly over the available data set, which complicates the target parameter estimation.

Our analysis gives sufficient conditions for the target parameter estimates to be consistent in the noiseless case, and this is shown to hold under mild conditions on the transmitted signal of opportunity. Next, we derive the covariance matrix of the target parameter estimates under the assumption of sufficiently small noise variances in both the reference and the surveillance channel. This is expressed as the sum of the Cramér-Rao lower bound for a noise-free reference signal, and a penalty term that explicitly captures the effect of noise in the reference channel. Based on this, we give an explicit sufficient condition for the effect of the reference channel noise to be negligible. The theoretical mean-square error calculations are compared with empirical results using Monte-Carlo simulations in some different scenarios. Some general conclusions are that the empirical MSE agrees well with theoretical predictions, and also that the conditions for the noise in the reference channel to be negligible is rather strict. We also found that the way data is divided into batches matters for the frame-based approach. Of the studied techniques, the sparse sampling approach was preferable to the consecutive sampling version. This, since the former has a much smaller loss of resolution due to the longer time duration in each batch. The effect can be mitigated by processing the different batches coherently, which, however, complicates a recursive implementation of the technique.

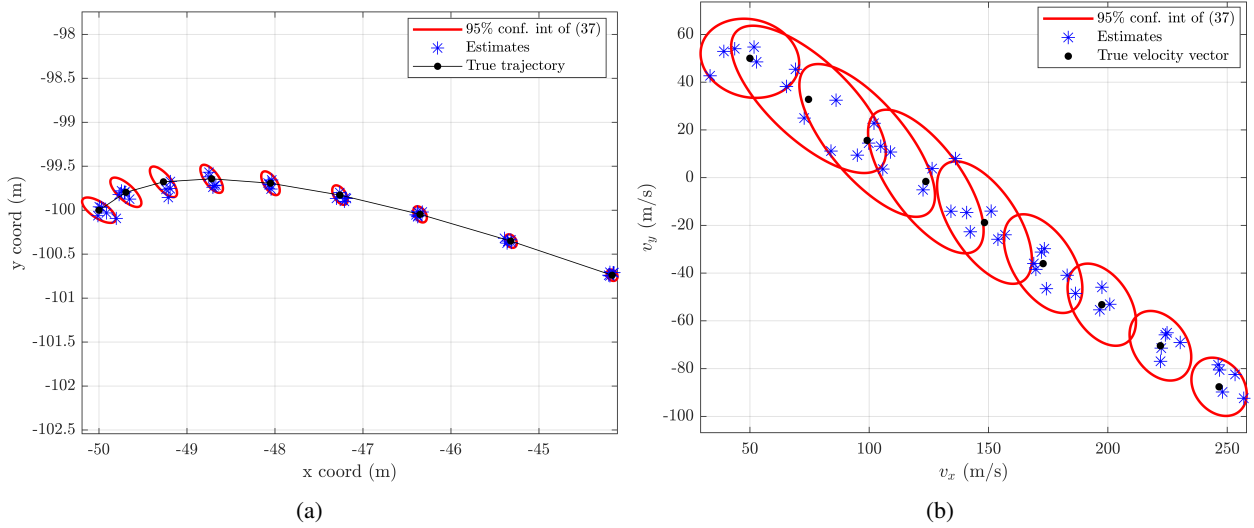


Fig. 5: Target tracking illustration.

APPENDIX A COVARIANCE MATRIX OF THE GRADIENT

The purpose of this appendix is to derive the term $\mathbb{E}[V'(\boldsymbol{\theta}_0)V'^T(\boldsymbol{\theta}_0)]$ appearing in (33). Clearly, from (20) with $w_k \equiv 1$ we have

$$V'(\boldsymbol{\theta}_0) = \sum_{k=1}^K P'_k(\boldsymbol{\theta}_0), \quad (41)$$

where we regard P_k as a function of $\boldsymbol{\theta}$, indirectly through the known functions $\tau_k(\boldsymbol{\theta})$ and $\omega_k(\boldsymbol{\theta})$. Alternatively, for a single node we let τ_k and ω_k be the parameters to be estimated. Let P'_k denote the derivative of P_k w.r.t. one of the components in $\boldsymbol{\theta}$. From (18) we have

$$P'_k(\boldsymbol{\theta}_0) = \mathbf{y}_k^H \hat{\mathbf{P}}' \mathbf{y}_k. \quad (42)$$

The projection matrix $\hat{\mathbf{P}}$ depends on $\boldsymbol{\theta}$ through the steering vector $\hat{\mathbf{a}}$, where the dependence on τ_k and ω_k has been suppressed. Applying the perturbation theory of projection matrices (e.g. [35], [36]) now yields

$$\begin{aligned} P'_k(\boldsymbol{\theta}_0) &= \mathbf{y}_k^H \left(\hat{\mathbf{P}}^\perp \hat{\boldsymbol{\Pi}}^\perp \hat{\mathbf{a}}' (\hat{\boldsymbol{\Pi}}^\perp \hat{\mathbf{a}})^+ + (\hat{\boldsymbol{\Pi}}^\perp \hat{\mathbf{a}})^+ H \hat{\mathbf{a}}' H \hat{\boldsymbol{\Pi}}^\perp \hat{\mathbf{P}}^\perp \right) \mathbf{y}_k \\ &= 2 \Re \left\{ \mathbf{y}_k^H \hat{\mathbf{P}}^\perp \hat{\boldsymbol{\Pi}}^\perp \hat{\mathbf{a}}' (\hat{\boldsymbol{\Pi}}^\perp \hat{\mathbf{a}})^+ \mathbf{y}_k \right\}, \end{aligned} \quad (43)$$

where $(\cdot)^+$ denotes the Moore-Penrose pseudo-inverse of a matrix and $\hat{\mathbf{P}}^\perp = \mathbf{I} - \hat{\mathbf{P}}$. In these expressions, it is understood that $\hat{\mathbf{a}}$ and its derivative $\hat{\mathbf{a}}' = \partial \hat{\mathbf{a}} / \partial \boldsymbol{\theta}$ should be evaluated at the true parameter vector $\boldsymbol{\theta}_0$. Next, we insert the expression for the received SC signal as

$$\mathbf{y}_k = \mathbf{y}_{I,k} + d_k \mathbf{a} + \mathbf{e}_k \quad (44)$$

$$\mathbf{y}_{I,k} = [\mathbf{s}_k, \mathbf{S}_k] \begin{bmatrix} b_k \\ \mathbf{c}_k \end{bmatrix} = \mathbf{S}_{I,k} \mathbf{f}_k \quad (45)$$

where $\mathbf{y}_{I,k}$ is the total interference component. In addition, a first-order expression for the interference cancelation matrix

$\hat{\boldsymbol{\Pi}}^\perp$ is needed. Arrange the RC signal and noise components conformably with $\mathbf{S}_{I,k}$ above, so that $\mathbf{X}_{I,k} = a_k \mathbf{S}_{I,k} + \mathbf{N}_{I,k}$. Assuming $\|\mathbf{N}_{I,k}\|$ to be much smaller than $\|a_k \mathbf{S}_{I,k}\|$ (in the mean-square sense), we have

$$\hat{\boldsymbol{\Pi}}^\perp \simeq \boldsymbol{\Pi}^\perp - \Delta \boldsymbol{\Pi}, \quad (46)$$

where $\boldsymbol{\Pi}^\perp$ is defined in (12), and the first-order perturbation term is given by

$$\Delta \boldsymbol{\Pi} = \boldsymbol{\Pi}^\perp \mathbf{N}_{I,k} (a_k \mathbf{S}_{I,k})^+ + (a_k \mathbf{S}_{I,k})^{+H} \mathbf{N}_{I,k}^H \boldsymbol{\Pi}^\perp. \quad (47)$$

In the approximation of (43) we will use that $\boldsymbol{\Pi}^\perp \mathbf{y}_{I,k} = 0$ and $(\boldsymbol{\Pi}^\perp \mathbf{a})^+ \mathbf{a} = 1$. Further, let

$$\mathbf{P} = \frac{\boldsymbol{\Pi}^\perp \mathbf{a} \mathbf{a}^H \boldsymbol{\Pi}^\perp}{\mathbf{a}^H \boldsymbol{\Pi}^\perp \mathbf{a}} = \mathbf{I} - \mathbf{P}^\perp$$

denote the projection matrix (19) onto the noise-free interference-canceled steering vector $\boldsymbol{\Pi}^\perp \mathbf{a}$. Both these factors are subject to perturbation, where $\Delta \boldsymbol{\Pi}$ is given in (47). Since $\hat{\mathbf{a}}$ is constructed from \mathbf{x}_k and not \mathbf{s}_k , we have $\hat{\mathbf{a}} \approx a_k \mathbf{a}$ and $\Delta \mathbf{a} = \hat{\mathbf{a}} - a_k \mathbf{a} = \mathbf{n}_k \odot \mathbf{v}(\omega_k)$. The first-order expression of $\hat{\mathbf{P}}$ is therefore obtained as

$$\hat{\mathbf{P}} = \mathbf{P} + \Delta \mathbf{P} \quad (48)$$

$$\Delta \mathbf{P} = \mathbf{P}^\perp (\boldsymbol{\Pi}^\perp \Delta \mathbf{a} - \Delta \boldsymbol{\Pi} a_k \mathbf{a}) (\boldsymbol{\Pi}^\perp a_k \mathbf{a})^+ \quad (49)$$

$$+ (\boldsymbol{\Pi}^\perp a_k \mathbf{a})^{+H} (\boldsymbol{\Pi}^\perp \Delta \mathbf{a} - \Delta \boldsymbol{\Pi} a_k \mathbf{a})^H \mathbf{P}^\perp. \quad (50)$$

We note, in passing, that both $\Delta \boldsymbol{\Pi}$ and $\Delta \mathbf{P}$ are of order $\sigma_n^2 / |a_k|^2$ in the mean-square sense, which we recognize as the Noise-to-Signal Ratio in the RC, as expected.

Inserting (44) – (50) into (43), we can split the gradient into the two components

$$P'_k(\boldsymbol{\theta}_0) \simeq T_1 + T_2 \quad (51)$$

where T_1 represents the first-order contribution from the noise in the SC, and T_2 contains the effect of the noise in the RC

channel. After some manipulations, which we omit, the terms are obtained as

$$T_1 = 2 \Re \left\{ \mathbf{e}_k^H \mathbf{P}^\perp \mathbf{\Pi}^\perp \mathbf{a}' d_k \right\} \quad (52)$$

and

$$T_2 = \frac{2}{a_k} \Re \left\{ (\mathbf{N}_{I,k} \mathbf{f}_{I,k} + \Delta \mathbf{a} d_k)^H \mathbf{P}^\perp \mathbf{\Pi}^\perp \mathbf{a}' d_k \right\} \quad (53)$$

respectively.

Given the first-order approximation of the gradient, we can now compute its approximate covariance matrix. Since the terms in (20) are independent, the covariance matrix can be computed for each term separately. Denote the first-order covariance matrix for the k :th node \mathbf{Q}_k . Its i, j :th element is then given by

$$\mathbf{Q}_k(i, j) = \mathbb{E} \left[\frac{\partial P_k(\boldsymbol{\theta})}{\partial \theta_i} \frac{\partial P_k(\boldsymbol{\theta})}{\partial \theta_j} \right] = T_1(i, j) + T_2(i, j). \quad (54)$$

where we have used that T_1 and T_2 are independent. To evaluate the covariance elements, let \mathbf{a}'_i denote the partial derivative of $\mathbf{a}(\tau_k, \omega_k)$ with respect to the target parameter θ_i , i.e.,

$$\mathbf{a}'_i = \frac{\partial \mathbf{a}(\tau_k(\boldsymbol{\theta}), \omega_k(\boldsymbol{\theta}))}{\partial \theta_i}.$$

We then have

$$T_1(i, j) = 4 \mathbb{E} \left[\Re \left\{ \mathbf{e}_k^H \mathbf{P}^\perp \mathbf{\Pi}^\perp \mathbf{a}'_i d_k \right\} \Re \left\{ \mathbf{e}_k^H \mathbf{P}^\perp \mathbf{\Pi}^\perp \mathbf{a}'_j d_k \right\} \right] \quad (55)$$

and

$$T_2(i, j) = \frac{4}{|a_k|^2} \mathbb{E} \left[\Re \left\{ (\mathbf{N}_I \mathbf{f}_I + \Delta \mathbf{a} d_k)^H \mathbf{\Pi}^\perp \mathbf{P}^\perp \mathbf{a}'_i d_k \right\} \cdot \Re \left\{ (\mathbf{N}_I \mathbf{f}_I + \Delta \mathbf{a} d_k)^H \mathbf{\Pi}^\perp \mathbf{P}^\perp \mathbf{a}'_j d_k \right\} \right]. \quad (56)$$

where we recall that $\Delta \mathbf{a} = \mathbf{n}_k \odot \mathbf{v}(\omega_k)$. In order to evaluate the expectations, use is made of the fact that if u and v are two complex scalars, it holds

$$2 \Re \{u\} \Re \{v\} = \Re \{uv\} + \Re \{uv^H\}.$$

Using this and that \mathbf{e}_k is circularly symmetric, (55) evaluates to

$$\begin{aligned} T_1(i, j) &= 2 |d_k|^2 \mathbb{E} \left[\Re \left\{ \mathbf{a}'_i^H \mathbf{\Pi}^\perp \mathbf{P}^\perp \mathbf{e}_k \mathbf{e}_k^H \mathbf{P}^\perp \mathbf{\Pi}^\perp \mathbf{a}'_j \right\} \right] \\ &= 2 |d_k|^2 \sigma_e^2 \Re \left\{ \mathbf{a}'_i^H \tilde{\mathbf{P}} \mathbf{a}'_j \right\}, \end{aligned} \quad (57)$$

where $\tilde{\mathbf{P}}$ is defined in (36).

Next, to evaluate $T_2(i, j)$, we recall that $\mathbf{N}_{I,k} = [\mathbf{n}_k, \mathbf{N}_k]$. Thus, we can rewrite the noise contribution as

$$\begin{aligned} \mathbf{N}_{I,k} \mathbf{f}_k + \Delta \mathbf{a} d_k &= \mathbf{N}_k \mathbf{c}_k + \mathbf{n}_k b_k + \mathbf{n}_k \odot \mathbf{v}(\omega_k) d_k \\ &= \mathbf{Z}_k \text{vec}(\mathbf{N}_{I,k}), \end{aligned}$$

where \mathbf{Z}_k is defined in (35). The matrix $\mathbf{N}_{I,k}$ is a Toeplitz matrix of the RC noise samples. Thus, we can write

$$\text{vec}(\mathbf{N}_{I,k}) = \mathbf{J}_k \mathbf{n}_{I,k},$$

where $\mathbf{n}_{I,k} = [n(-L), n(-L+1), \dots, n(N-1)]^T$ is the vector of all noise samples, and where \mathbf{J}_k is a selection matrix that picks out the respective component from $\mathbf{n}_{I,k}$. This leads to

$$\mathbf{N}_I \mathbf{f}_I + \Delta \mathbf{a} d_k = \mathbf{Z}_k \mathbf{J}_k \mathbf{n}_{I,k}. \quad (58)$$

Inserting (58) into (56) now leads to

$$T_2(i, j) = 2 |d_k|^2 \frac{\sigma_n^2}{|a_k|^2} \Re \left\{ \mathbf{a}'_i^H \tilde{\mathbf{P}} \mathbf{Z}_k \mathbf{J}_k \mathbf{J}_k^T \mathbf{Z}_k^H \tilde{\mathbf{P}} \mathbf{a}'_j \right\}. \quad (59)$$

Collecting the partial derivatives of \mathbf{a} into the matrix

$$\mathbf{D} = [\mathbf{a}'_1, \dots, \mathbf{a}'_4], \quad (60)$$

and inserting (57) and (59) into (54), we can express the asymptotic covariance matrix of the gradient as

$$\begin{aligned} \mathbf{Q}_k &= 2 |d_k|^2 \sigma_e^2 \Re \left\{ \mathbf{D}^H \tilde{\mathbf{P}} \mathbf{D} \right\} \\ &\quad + 2 |d_k|^2 \frac{\sigma_n^2}{|a_k|^2} \Re \left\{ \mathbf{D}^H \tilde{\mathbf{P}} \mathbf{Z}_k \mathbf{J}_k \mathbf{J}_k^T \mathbf{Z}_k^H \tilde{\mathbf{P}} \mathbf{D} \right\}. \end{aligned} \quad (61)$$

The two terms represent the contributions from the noise in the SC and in the RC respectively. Finally, adding all terms as in (41), we arrive at

$$\mathbb{E}[V'(\boldsymbol{\theta}_0) V'^T(\boldsymbol{\theta}_0)] = \sum_{k=1}^K \mathbf{Q}_k. \quad (62)$$

APPENDIX B ASYMPTOTIC HESSIAN MATRIX

For the asymptotic Hessian matrix we set $\sigma_n^2 + \sigma_e^2 = 0$ and differentiate the projection matrix in (18) accordingly. We set $\mathbf{b} = \mathbf{\Pi}^\perp \mathbf{a}$ and follow the calculations outlined in Appendix B of [36]. As above, we use the notation $\partial_i \mathbf{b} / \partial \theta_i = \mathbf{b}'_i$, and further $\partial^2 \mathbf{b} / \partial \theta_i \partial \theta_j = \mathbf{b}''_{ij}$. We have already seen in (43) that

$$\mathbf{P}'_i = \mathbf{b}'_i \mathbf{b}^+ + \mathbf{b}(\mathbf{b}_i^+)' = \mathbf{P}^\perp \mathbf{b}'_i \mathbf{b}^+ + (\mathbf{P}^\perp \mathbf{b}'_i \mathbf{b}^+)^H, \quad (63)$$

while the second derivatives are obtained as in [36]

$$\begin{aligned} \mathbf{P}''_{ij} &= -\mathbf{P}^\perp \mathbf{b}'_j \mathbf{b}^+ \mathbf{b}'_i \mathbf{b}^+ - (\mathbf{b}^+)^H (\mathbf{b}'_j)^H \mathbf{P}^\perp \mathbf{b}'_i \mathbf{b}^+ + \mathbf{P}^\perp \mathbf{b}''_{ij} \mathbf{b}^+ \\ &\quad + \mathbf{P}^\perp \mathbf{b}'_i (\mathbf{b}'_j)^H \mathbf{P}^\perp / \|\mathbf{b}\|^2 - \mathbf{P}^\perp \mathbf{b}'_i \mathbf{b}^+ \mathbf{b}'_i \mathbf{b}^+ + (\dots)^H. \end{aligned} \quad (64)$$

where $(\dots)^H$ means the Hermitian transpose of all the previous terms. Now we need to understand the interplay between the latter and the vectors \mathbf{y}_k , when computing the quadratic form $\mathbf{y}_k^H \mathbf{P}''_{ij} \mathbf{y}_k$. The key observation is that all the \mathbf{b}'_i still belong to $\text{span}(\mathbf{\Pi}^\perp)$, because $\mathbf{\Pi}^\perp$ does not depend on the parameters $\boldsymbol{\theta}$. Moreover, we also need to recall that $\mathbf{y}_k = \mathbf{g}_k + d_k \mathbf{a}_k$ for some $\mathbf{g}_k \in \text{span}(\mathbf{S}_I)$; thus $\mathbf{y}_k^H \mathbf{P}^\perp = \mathbf{y}_k^H (\mathbf{I} - \mathbf{P}) = \mathbf{y}_k^H - (\mathbf{P} \mathbf{y}_k)^H = \mathbf{g}_k^H$ and by $\mathbf{g}_k \perp \mathbf{b}'_i$, we can conclude that all the factors in (64) beginning with $\mathbf{P}^\perp \mathbf{b}'_i$ vanish when left-multiplied by \mathbf{y}_k^H . Similarly for $(\dots)^H$. Therefore, by using $\mathbf{b}^+ = \mathbf{b}^H / \|\mathbf{b}\|^2$ and $\mathbf{b}^H \mathbf{a} = \|\mathbf{b}\|^2$, we obtain

$$\mathbf{y}_k^H \mathbf{P}''_{ij} \mathbf{y}_k = -2 |d_k|^2 \Re \left\{ (\mathbf{b}'_j)^H \mathbf{P}^\perp \mathbf{b}'_i \right\}. \quad (65)$$

Note that (65) equals (57) up to a multiplicative factor as expected. The above can be put into matrix form as

$$\mathbf{H}_k = -2 |d_k|^2 \Re \left\{ \mathbf{D}^H \tilde{\mathbf{P}} \mathbf{D} \right\}. \quad (66)$$

Inserting (61) and (66) into (33), including the contributions from all receiving nodes, we finally arrive at

$$\mathbb{E}[(\hat{\theta} - \theta_0)(\hat{\theta} - \theta_0)^T] \approx \mathbf{H}^{-1} \mathbf{Q} \mathbf{H}^{-1} \quad (67)$$

with

$$\mathbf{H} = -2 \sum_{k=1}^K |d_k|^2 \Re \{ \mathbf{D}_k^H \tilde{\mathbf{P}}_k \mathbf{D}_k \} \quad (68)$$

and \mathbf{Q} as in (62).

APPENDIX C CONSISTENCY DISCUSSION

Before proving Theorem 1, we need to recall a technical result from [37]:

Proposition C.1 (6.11 in [37]). *Let $\mathcal{Y} = \{Y(t) : t \in W\}$ be a random field with values in \mathbb{R}^{m+k} and $W \subseteq \mathbb{R}^d$ open. Let $u \in \mathbb{R}^{m+k}$ and I a subset of W . We assume that \mathcal{Y} satisfies the following conditions:*

- the paths $t \rightsquigarrow Y(t)$ are of class \mathcal{C}^1 ,
- for each $t \in W$, the random vector $Y(t)$ has a density, and there exists a constant C such that $p_{Y(t)}(x) \leq C$ for $t \in I$ and x is some neighborhood of u ,
- the Hausdorff dimension of I is smaller or equal than m .

Then, almost surely, there is no point $t \in I$ such that $Y(t) = u$.

Proof of Theorem 1. We assume without loss of generality that $\tau_0 = \omega_0 = 0$. Observe also that $\mathbf{v} \neq \mathbf{0}$ almost surely. The event in (30) is equivalent to $\{\exists (\tau, \omega, \alpha) \in T \times \mathbb{C} : \mathbf{w}(\tau, \omega) + \alpha \mathbf{v} = 0\}$; therefore we consider the Gaussian non-stationary random field $\mathbf{h} : \mathbb{R}^4 \rightarrow \mathbb{R}^{2N}$ defined by

$$(\tau, \omega, \alpha_1, \alpha_2)^T \mapsto (\Re(\mathbf{w}(\tau, \omega)_1 + \alpha \mathbf{v}_1), \dots, \Re(\mathbf{w}(\tau, \omega)_N + \alpha \mathbf{v}_N), \Im(\mathbf{w}(\tau, \omega)_1 + \alpha \mathbf{v}_1), \dots, \Im(\mathbf{w}(\tau, \omega)_N + \alpha \mathbf{v}_N))^T$$

where we use the identification $\alpha = \alpha_1 + j\alpha_2 \cong (\alpha_1, \alpha_2)$. The goal is to show that the hypotheses of Proposition 6.11 in [37] (that we reported as Proposition C.1 for convenience) hold for \mathbf{h} . This would imply that the level set $\{\mathbf{w}(\tau, \omega) + \alpha \mathbf{v} = 0\}$ is almost surely empty.

As an immediate consequence of the hypothesis on s (cf. Theorem 11 in [38]) and on the structure of \mathbf{h} , we have that the paths of each component of \mathbf{h} are at least of class \mathcal{C}^1 .

Since \mathbf{h} is Gaussian, to show that \mathbf{h} has a density it suffices to show its covariance matrix is nonsingular. We can factor \mathbf{h} in a more convenient way: $\mathbf{h}(\tau, \omega, \alpha) = \mathbf{B}(\omega, \alpha) \mathbf{x}(\tau)$ where

$$\mathbf{x}(\tau) = (\Re(s(t_1 - \tau)), \Im(s(t_1 - \tau)), \dots, \Re(s(t_N - \tau)), \Im(s(t_N - \tau)), \Re(s(t_1)), \Im(s(t_1)), \dots, \Re(s(t_N)), \Im(s(t_N)))^T \in \mathbb{R}^{4N},$$

and $\mathbf{B}(\omega, \alpha) = (\mathbf{R}(\omega) \quad \mathbf{A}(\alpha))$ is a $2N \times 4N$ matrix with real entries, and both $\mathbf{R}(\omega)$ and $\mathbf{A}(\alpha)$ are $2N \times 2N$ block diagonal matrices whose blocks are

$$\begin{pmatrix} \cos(\omega t_n) & -\sin(\omega t_n) \\ \sin(\omega t_n) & \cos(\omega t_n) \end{pmatrix}, \quad n = 1, \dots, N$$

for $\mathbf{R}(\omega)$ and

$$\begin{pmatrix} \alpha_1 & -\alpha_2 \\ \alpha_2 & \alpha_1 \end{pmatrix}$$

for $\mathbf{A}(\alpha)$. From this form, it is straightforward to see that $\mathbf{B}(\omega, \alpha)$ has full row rank for all ω and α . The covariance matrix $\Sigma_{\mathbf{h}}(\tau, \omega, \alpha)$ of \mathbf{h} can then be expressed as

$$\Sigma_{\mathbf{h}}(\tau, \omega, \alpha) = \mathbf{B}(\omega, \alpha) \Sigma_{\mathbf{x}}(\tau) \mathbf{B}(\omega, \alpha)^T,$$

and to prove its non-singularity it is enough to prove that $\Sigma_{\mathbf{x}}(\tau)$ is non-singular.

Introduce the auxiliary complex-valued $2N$ -vector

$$\mathbf{z}(\tau) = (s(t_1 - \tau), \dots, s(t_N - \tau), s(t_1), \dots, s(t_N))^T \in \mathbb{C}^{2N}.$$

Then $\mathbf{x}(\tau)$ equals $(\Re(\mathbf{z}(\tau))^T, \Im(\mathbf{z}(\tau))^T)^T$, up to a permutation matrix P . In particular, $\Sigma_{\mathbf{x}}(\tau)$ is non-singular if $\Sigma_{\mathbf{z}}(\tau)$ is so, because s is circularly symmetric with real even spectral density, where $\Sigma_{\mathbf{z}}(\tau) = \mathbb{E}[\mathbf{z}(\tau) \mathbf{z}(\tau)^H]$. Because $\Sigma_{\mathbf{z}}(\tau)$ is a covariance matrix, it is positive semi-definite. Therefore, to prove that it is non-singular it is sufficient to show that

$$\mathbf{c}^H \Sigma_{\mathbf{z}}(\tau) \mathbf{c} = 0 \implies \mathbf{c} = \mathbf{0} \in \mathbb{C}^{2N}.$$

By the Wiener-Khinchin Theorem, we can write

$$\begin{aligned} \mathbf{c}^H \Sigma_{\mathbf{z}}(\tau) \mathbf{c} &= \sum_{n, \ell} \overline{c_n} c_\ell \mathbb{E}[\mathbf{z}(\tau)_n \overline{\mathbf{z}(\tau)_\ell}] \\ &= \sum_{n, \ell} \int_{\mathbb{R}} \overline{c_n} c_\ell e^{jf(u_n - u_\ell)} \mathcal{S}_s(f) df \\ &= \int_{\mathbb{R}} \left(\sum_n \overline{c_n} e^{jf u_n} \right) \left(\sum_\ell c_\ell e^{-jf u_\ell} \right) \mathcal{S}_s(f) df \\ &= \int_{-B/2}^{B/2} \left| \sum_{n=1}^{2N} c_n e^{-jf u_n} \right|^2 df, \end{aligned} \quad (69)$$

where $u_n \in \{t_1 - \tau, t_2 - \tau, \dots, t_N - \tau, t_1, \dots, t_N\}$. Since the complex exponentials $\{e^{-jf u_n}\}_{n=1}^{2N}$, viewed as functions of f , are linearly independent over \mathbb{C} , for any $\mathbf{c} \neq \mathbf{0}$, the function $f \mapsto \left| \sum_{n=1}^{2N} c_n e^{-jf u_n} \right|^2$ is not identically zero. By a continuity argument, it is therefore strictly positive on a set of positive Lebesgue measure. This holds as long as the u_n are all distinct, which happens if and only if $\tau \neq t_p - t_q$ for $t_p, t_q \in \{t_1, \dots, t_N\}$, since we have assumed $t_p \neq t_q$ for $p \neq q$, and the only possible collisions are cross-collisions of the form $t_p - \tau = t_q$. This shows that $\Sigma_{\mathbf{z}}(\tau)$ (and thus $\Sigma_{\mathbf{x}}(\tau)$) is non-singular for all $\tau \notin T_1 = \{0\} \cup \bigcup_{p \neq q} \{t_p - t_q\}$. It follows that \mathbf{h} has a density for all $(\tau, \omega, \alpha) \in (\mathbb{R} \setminus T_1) \times \mathbb{R}^3$.

The argument outlined so far proves that the Gaussian density for \mathbf{h} exists, but to show that also the second part of the second requirement of Proposition C.1 is fulfilled, we need to establish a uniform bound on the eigenvalues of $\Sigma_{\mathbf{h}}$ with respect to all parameters.

A first observation concerns $\Sigma_{\mathbf{x}}$. The map $\tau \mapsto \lambda_{\min}(\Sigma_{\mathbf{x}}(\tau))$ is continuous and strictly positive on $\mathbb{R} \setminus T_1$. Hence, for any fixed compact set $T_3 \subset \mathbb{R} \setminus T_1$, it attains its

minimum on T_3 ; in particular, there exists $c_{T_3} > 0$ such that $\lambda_{\min}(\Sigma_{\mathbf{X}}(\tau)) \geq c_{T_3}$ for all $\tau \in T_3$. Notice that T_3 can be selected to be a finite union of disjoint closed intervals.

With this at hand, we can observe that, since the matrix \mathbf{B} has orthogonal rows with $\mathbf{B}(\omega, \alpha)\mathbf{B}(\omega, \alpha)^T = (1 + |\alpha|^2)\mathbf{I}_{2N}$,

$$\begin{aligned} \lambda_{\min}(\Sigma_{\mathbf{h}}(\tau, \omega, \alpha)) &\geq (1 + |\alpha|^2)\lambda_{\min}(\Sigma_{\mathbf{X}}(\tau)) \\ &\geq \lambda_{\min}(\Sigma_{\mathbf{X}}(\tau)) \end{aligned} \quad (70)$$

as a consequence of the Poincaré separation theorem. The last term of (70) is uniformly bounded away from 0, provided that $(\tau, \omega, \alpha) \in T \times \mathbb{R}^2$, where we set $T = T_3 \times \mathbb{R}$. Therefore, we conclude by applying Proposition C.1 with $I = T \times \mathbb{R}^2 \subset \mathbb{R}^4$, $m = 4$, $k = 2N - 4$, so that the Hausdorff dimension $\dim_H(I) \leq 4 = m$. \square

REFERENCES

- [1] H. Kuschel, "Passive coherent locator history and fundamentals," *STO, NATO Science and Technology Organization*, 2017.
- [2] F. J. Yanovsky, A. I. Nosich, O. O. Drobakhin, A. A. Shramkova, N. T. Cherpak, Y. A. Averyanova, K. Arkhypova, and D. M. Vavriv, "Microwave activities in Ukraine," *2019 European Microwave Conference in Central Europe (EuMCE)*, pp. 229–234, 2019.
- [3] L. Jun, H. Li, and B. Himed, "Two Target Detection Algorithms for Passive Multistatic Radar," *IEEE Transactions on Signal Processing*, vol. 62, no. 22, pp. 5930–5939, 2014.
- [4] D. Cochran, H. Gish, and D. Sino, "A Geometric Approach to Multiple-Channel Signal Detection," *IEEE Transactions on Signal Processing*, vol. 43, no. 9, pp. 2049–2057, 1995.
- [5] S. D. Howard, S. Sirianupiboon, and D. Cochran, "An exact Bayesian detector for multistatic passive radar," *2016 50th Asilomar Conference on Signals, Systems and Computers*, pp. 1077–1080, 2016.
- [6] S. D. Howard and S. Sirianupiboon, "Passive radar detection using multiple transmitters," *2013 Asilomar Conference on Signals, Systems and Computers*, pp. 945–948, 2013.
- [7] Q. Zhou, Y. Yuan, H. Li, M. S. Greco, F. Gini, and W. Yi, "Direct localization with direct-path interference for reference channel-free distributed passive radars," *IEEE Transactions on Signal Processing*, vol. 73, pp. 4379–4396, 2025.
- [8] J. Wei, J. Li, C. Song, Z. Xu, and K. Ding, "An adaptive fusion algorithm for multistatic and multichannel passive radar detection," *2021 IEEE Radar Conference (RadarConf21)*, pp. 1–6, 2021.
- [9] F. Colone, D. W. O'Hagan, P. Lombardo, and C. J. Baker, "A Multistage Processing Algorithm for Disturbance Removal and Target Detection in Passive Bistatic Radar," *IEEE Trans. Aerosp. Electron. Syst.*, vol. 45, no. 2, pp. 698–722, 2009.
- [10] Q. Zhou, Y. Yuan, L. Venturino, and W. Yi, "Direct Target Localization for Distributed Passive Radars With Direct-Path Interference Suppression," *IEEE Trans. Signal Process.*, vol. 72, pp. 3611–3625, 2024.
- [11] X. Zhang, H. Li, and B. Himed, "Maximum Likelihood Delay and Doppler Estimation for Passive Sensing," *IEEE Sensors J.*, vol. 19, pp. 180–188, Jan. 2019.
- [12] S. Thomopoulos, R. Viswanathan, and D. Bougoulias, "Optimal distributed decision fusion," *IEEE Trans. Aerosp. Electron. Syst.*, vol. 25, pp. 761–765, Sept. 1989.
- [13] A. Tajer, G. H. Jajamovich, X. Wang, and G. V. Moustakides, "Optimal Joint Target Detection and Parameter Estimation by MIMO Radar," *IEEE J. Sel. Top. Signal Process.*, vol. 4, no. 1, pp. 127–145, 2010.
- [14] W. Yi, T. Zhou, Y. Ai, and R. S. Blum, "Suboptimal Low Complexity Joint Multi-Target Detection and Localization for Non-Coherent MIMO Radar With Widely Separated Antennas," *IEEE Trans. Signal Process.*, vol. 68, pp. 901–916, 2020.
- [15] Q. He, R. S. Blum, and A. M. Haimovich, "Noncoherent MIMO Radar for Location and Velocity Estimation: More Antennas Means Better Performance," *IEEE Trans. Signal Process.*, vol. 58, pp. 3661–3680, July 2010.
- [16] M. S. Greco, P. Stinco, F. Gini, and A. Farina, "Cramer-Rao Bounds and Selection of Bistatic Channels for Multistatic Radar Systems," *IEEE Trans. Aerosp. Electron. Syst.*, vol. 47, pp. 2934–2948, Oct. 2011.
- [17] A. Liu, Z. Huang, M. Li, Y. Wan, W. Li, T. X. Han, C. Liu, R. Du, D. K. P. Tan, J. Lu, Y. Shen, F. Colone, and K. Chetty, "A survey on fundamental limits of integrated sensing and communication," *IEEE Communications Surveys & Tutorials*, vol. 24, no. 2, pp. 994–1034, 2022.
- [18] J. Tong, H. Gaoming, T. Wei, and P. Huafu, "Cramér-rao lower bound analysis for stochastic model based target parameter estimation in multistatic passive radar with direct-path interference," *IEEE Access*, vol. 7, pp. 106761–106772, 2019.
- [19] J. L. Garry, C. J. Baker, and G. E. Smith, "Evaluation of direct signal suppression for passive radar," *IEEE Transactions on Geoscience and Remote Sensing*, vol. 55, no. 7, pp. 3786–3799, 2017.
- [20] J. E. Palmer and S. J. Searle, "Evaluation of adaptive filter algorithms for clutter cancellation in passive bistatic radar," in *2012 IEEE Radar Conference*, pp. 0493–0498, 2012.
- [21] Y. Ma, T. Shan, Y. D. Zhang, M. G. Amin, R. Tao, and Y. Feng, "A novel two-dimensional sparse-weight nlms filtering scheme for passive bistatic radar," *IEEE Geoscience and Remote Sensing Letters*, vol. 13, no. 5, pp. 676–680, 2016.
- [22] X. Bai, J. Han, J. Zhao, Y. Feng, and R. Tao, "Clutter cancellation in passive radar using batch-based CLEAN technique," *EURASIP Journal on Advances in Signal Processing*, vol. 63, 2021.
- [23] X. Lyu and Y. Ding, "Joint multipath signals and noise reduction in passive radar," *IET Signal Processing*, vol. 16, pp. 366–376, 2022.
- [24] "Fast and efficient clutter cancellation approach for dvb-t based passive radars," *Progress In Electromagnetics Research B*, vol. 98, pp. 165–187, 2023.
- [25] Y. Guo, J. Geng, X. Zhang, and H. Dong, "Zero-doppler clutter suppression for drm-based passive radar under block fading channel via regularized eca-c," *Digital Signal Processing*, vol. 160, p. 105056, 2025.
- [26] Y. Du and P. Wei, "An explicit solution for target localization in noncoherent distributed mimo radar systems," *IEEE Signal Processing Letters*, vol. 21, no. 9, pp. 1093–1097, 2014.
- [27] W. C. Barott and J. Engle, "Single-antenna ATSC passive radar observations with remodulation and keystone formatting," in *2014 IEEE Radar Conference*, (Cincinnati, OH, USA), pp. 0159–0163, IEEE, May 2014.
- [28] T. Martelli, F. Filippini, F. Pignol, F. Colone, and R. Cardinali, "Computationally effective range migration compensation in pcl systems for maritime surveillance," in *2018 IEEE Radar Conference (RadarConf18)*, pp. 1406–1411, 2018.
- [29] J. Liu, H. Li, and B. Himed, "GLRT detection with unknown noise power in passive multistatic radar," in *2015 IEEE International Conference on Acoustics, Speech and Signal Processing (ICASSP)*, (South Brisbane, Queensland, Australia), pp. 5570–5574, IEEE, 2015.
- [30] M. Malanowski and K. Kulpa, "Two methods for target localization in multistatic passive radar," *IEEE Transactions on Aerospace and Electronic Systems*, vol. 48, no. 1, pp. 572–580, 2012.
- [31] K. Ho and W. Xu, "An accurate algebraic solution for moving source location using tdoa and fdoa measurements," *IEEE Transactions on Signal Processing*, vol. 52, no. 9, pp. 2453–2463, 2004.
- [32] M. Boutin and G. Kemper, "Global positioning: The uniqueness question and a new solution method," *Advances in Applied Mathematics*, vol. 160, p. 102741, 2024.
- [33] S. Kay, *Fundamentals of Statistical Signal Processing: Estimation Theory*. Englewood Cliffs, NJ: Prentice-Hall International Editions, 1998.
- [34] M. Viberg, D. Gerosa, T. McKelvey, and T. Eriksson, "Statistical analysis of target parameter estimation using passive radar," in *Proc. 10th Int'l Conf. Computational Advances in Multi-Sensor Adaptive Processing*, (Dominican Republic), IEEE, 2025. To Appear.
- [35] G. Golub and V. Pereyra, "The Differentiation of Pseudo-Inverses and Nonlinear Least Squares Problems Whose Variables Separate," *SIAM J. Num. Anal.*, vol. 10, pp. 413–432, 1973.
- [36] M. Viberg and B. Ottersten, "Sensor array processing based on subspace fitting," *IEEE Trans. on Signal Process.*, vol. 39, no. 5, pp. 1110–1121, 1991.
- [37] J.-M. Azaïs and M. Wschebor, *Level Sets and Extrema of Random Processes and Fields*. Wiley, 2009.
- [38] Y. K. Belyaev, "Local properties of the sample functions of stationary gaussian processes," vol. 5, no. 1, pp. 117–123, 1960.